ISSN(Online): 2319 - 8753
ISSN (Print) :2347 - 6710

International Journal of Innovative Research in Science, Engineering and Technology

(An ISO 3297: 2007 Certified Organization)

Vol. 4, Issue 2, February 2015

Design of a Novel Intelligent Damping Controller for UPFC in Power System Connected Offshore Wind Power Applications

Whei-Min Lin [1], Kai-Hung Lu [2]

Professor, Department of Electrical Engineering, National Sun Yat-Sen University, Kaohsiung, Taiwan [2]

PhD. Student, Department of Electrical Engineering, National Sun Yat-Sen University, Kaohsiung, Taiwan[1]

ABSTRACT: This paper proposes a unified power flow controller (UPFC)-based oscillation damping controller for use with a permanent magnet synchronous generator (PMSG)-based offshore wave farm (OWF). A novel intelligent damping controller (NIDC) was used to increase the stability of power control and improve the performance, where the proposed NIDC consists of the adaptive critic network, the Functional Link based Elman Neural Network (FLENN), and PID linear damping controller. The UPFC is used with the NIDC to OWF, which is connected to a single-machine infinite-bus to improve system stability. The PID damping controller is analysis of complex eigenvalues based on a theory of modal control. The node connecting weights of the FLENN and critic network are trained online. The proposed NIDC can be used to achieve better damping characteristics. The internal power fluctuations in the power system can also be effectively alleviated under variable wind power generation.

KEYWORDS: unified power flow controller (UPFC), Functional Link based Elman Neural Network (FLENN), offshore wave farm (OWF), PM synchronous generators (PMSG).

I. INTRODUCTION

Wind energy systems are attracting considerable attention as clean and safe sources of renewable power. Among the types of generator used for wind turbines, technical developments have moved from fixed-speed to variable-speed designs [1]. In recent years some small-scale offshore wind farms (OWFs) have been evaluated, while a number of large-scale OWFs have been constructed and are now in commercial operation. Researchers have examined induction generators with wound-rotor or cage-type rotors [2], [3], but in recent years there has been increasing interest in Permanent Magnet Synchronous Generators (PMSG). Such generators are attractive due to their compact structure, high air–gap flux density, high power density, high torque-to-inertia ratio, and high torque capability [4]. When OWFs deliver a large amount of electric power to power grids, the inherent power fluctuations that occur can have adverse impacts on the power quality of the systems to which they are connected. This paper thus proposes the use of a unified power flow controller (UPFC) in order to reduce the power fluctuations of large-scale grid-connected wind farms.

The UPFC proposed by Dr. Gyugyiin 1991, is the most flexible and powerful Flexible AC Transmission Systems (FACTS) device [5]-[8], which can provide an effective means to control the power flow, voltage and damping, and thus improve the transient stability of a power network. In the control of a UPFC series branch, both the active and reactive power flows in the transmission line are influenced through the series injected voltage as well as its phase angle [7], [8]. A fixed-parameter controller with classical control may thus not be effective for a UPFC [8], [9]. In such cases a flexible controller may be required, such as one based on neural networks [6], PSO [10] and robust control methodologies [11], in order to cope with system uncertainties and enhance the damping performance of a UPFC.

The Elman neural network (ENN) is a partially recurrent network model that was first proposed in 1990 [12]. The ENN is better than a static feed-forward network, and thus is widely applied with dynamic systems, although its convergence and training speed are usually very slow, and this it is not suitable for complex systems. In order to improve the ability to identify complex dynamic systems, a functional-link neural network (FLNN) is adopted in this paper to improve the performance of the ENN. This improved performance is because the input variables are linearly independent trigonometric basis functions which are used for a functional expansion of the FLNN in the extended space for classification. Moreover, the FLNN can capture the nonlinearly input–output relationships among a suitable

ISSN(Online): 2319 - 8753
ISSN (Print) :2347 - 6710

International Journal of Innovative Research in Science, Engineering and Technology

(An ISO 3297: 2007 Certified Organization)

Vol. 4, Issue 2, February 2015

set of polynomial inputs, since the high-order effects are incorporated in the input variables into higher dimensions of the input space. The FLNN can thus effectively approximate a nonlinear function [13], and so it is suitable to be applied in complex power system applications, such as the one examined in this work.

This paper proposed the design of a novel intelligent damping controller (NIDC) consists of a PID linear controller, functional link-based Elman Neural Network (FLENN) and critic network for a UPFC damping controller. The PID linear controller is analysis of complex eigenvalues based on a theory of modal control. An FLENN is unlike conventional controllers, the performances of which degrade for such changes and require retuning to produce the desired performance. The integrated OWF with a synchronous generators (SG) system is studied under the conditions of changes in wind speed, a three-phase short circuit fault and the transient responses. An NIDC is proposed in this work to achieve simultaneous power flow control and stability improvement.

II. ANALYSIS OF SYSTEM MODELS

Fig. 1 shows the configuration of the system studied in this paper. The OWF represented by a large equivalent aggregated PMSG is driven by an equivalent aggregated wind turbine through the gearbox in [2]. The SG with a capacity of 555MVA is connected to a single-machine infinite-bus (SMIB) through a transformer T_1 and two parallel transmission lines: Line 1 and Line 2. Line 2 contains the proposed UPFC located near Bus S. The aggregated OWF containing 200MW PMSG-based wind turbine generators is connected to Bus S through a T_2 transformer and a 15 km transmission cable. The equivalent wind PMSG is driven by an equivalent wind turbine through an equivalent gearbox. The employed capacity of the proposed UPFC is 160 MVA, and its series voltage is added to Bus S voltage V_S by the series connected transformer T_{se}. The shunt converter of the UPFC connected in shunt with the AC power system via a shunt transformer T_{sh} is primarily used to provide the real power demand of the series converter at the common DC link.

A. Wind Turbine Characteristics

The wind turbine input is the variable wind and the output is the mechanical power turning the generator rotor blades [4], [15].The output mechanical power available from a wind turbine can be obtained by

$$P_m = 0.5\rho \cdot V_\omega^3 \cdot A \cdot C_p(\lambda, \beta) \tag{1}$$

where ρ (kg/m^3) and A (m^2) are the air density and the area of turbine swept, respectively. V_ω is the wind velocity (m/sec), and C_p is the power performance coefficient, and is given as a nonlinear function of the tip speed ratio $T = \omega_r r / V_\omega$. ω_r is the turbine speed of blade radius r. C_p is a function of the T and the blade pitch angle β, and is generally defined with [4]

$$C_p = C_{p1}\left(\frac{C_{p2}}{T_i} - C_{p3} \cdot \beta - C_{p4} \cdot \beta^{C_{p5}} - C_{p6}\right) e^{\frac{-C_{p7}}{T_i}} \tag{2}$$

$$T_i = \frac{1}{\frac{1}{T - C_{p8}\beta} - \frac{C_{p9}}{\beta^3 + 1}} \tag{3}$$

where C_{p1} to C_{p9} are the wind turbine constant coefficients of C_p

B. PMSG

The wind generator chosen for this study is a three-phase PMSG, where the mechanical torque (T_m), electrical torque (T_e) and dynamic equation can be found in [4]. The machine model of a PMSG can be described in the rotor rotating reference frame as follows [4]

$$v_{qs} = Ri_q + d\Lambda_q/dt + \omega_s \Lambda_d \tag{4}$$

$$v_{ds} = Ri_d + d\Lambda_d/dt + \omega_s \Lambda_q \tag{5}$$

and

$$\Lambda_q = L_q i_q \tag{6}$$

$$\Lambda_d = L_d i_d + L_{md} I_{fd} \tag{7}$$

$$\omega_s = n_p \omega_r \tag{8}$$

where v_{ds}, v_{qs}, i_d, i_q, L_d, L_q, Λ_d and Λ_q are the d-q axis stator voltages, stator currents, inductances and the stator flux linkages, respectively. R is the stator resistance; ω_s is the rotational speed of inverter frequency; I_{fd} the equivalent d-axis magnetizing current; and L_{md} is the d-axis mutual inductance.

ISSN(Online): 2319 - 8753
ISSN (Print) :2347 - 6710

International Journal of Innovative Research in Science, Engineering and Technology

(An ISO 3297: 2007 Certified Organization)

Vol. 4, Issue 2, February 2015

The configuration of a field-oriented PMSG system consists of PMSG, a current-controlled PWM voltage source converter (VSC) and; vnverter (VSI), a field-orientation mechanism, including the coordinate translator, and a speed control loop. The input and output *d*, *q* axis voltages of VSC and VSI of wind PMSG could be expressed as

$$V_{vscd} = m_{vscd} \cdot v_{vscd} \cdot u_{dc};\ V_{vscq} = m_{vscq} \cdot v_{vscq} \cdot u_{dc} \quad (9)$$

$$V_{vsid} = m_{vsi} \cdot v_{ds}\, sin(\delta_{vsi});\ V_{vsiq} = m_{vsi} \cdot v_{ds}\, cos(\delta_{vsi}) \quad (10)$$

where u_{dc} is the dc link voltage; m_{vscd}, m_{vscq} and m_{vsi} are the *d*, *q* axis modulation indices of the VSC and VSI. δ_{vsi} is the phase angle of the VSI.

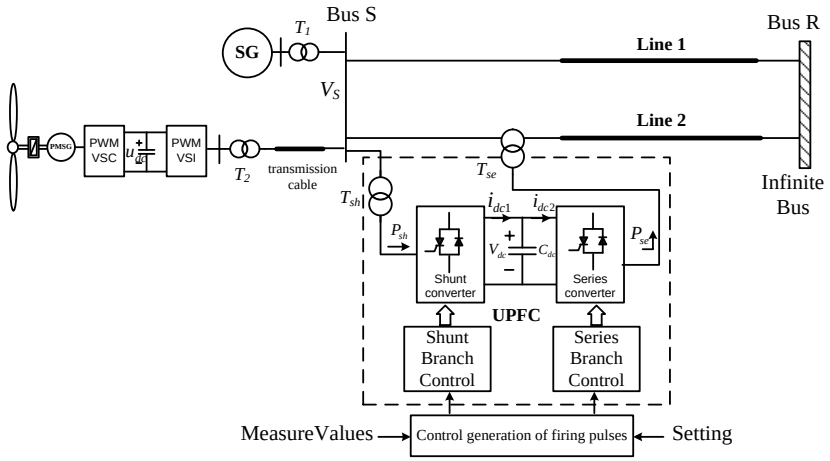

Fig. 1. Configuration of a UPFC system with the studied power system of a wind PMSG

C. Modeling of the UPFC

The UPFC consists of two voltage sourced converters, as illustrated in Fig. 1, the "Shunt Converter" and "Series Converter" operated from a common dc voltage, V_{dc} supported through a dc capacitor bank, C_{dc}. In the UPFC system, the series converter produces the inserted compensation voltage V_{se} in series with the transmission line, with the can be controlled magnitude from $V_{se,min}$ to $V_{se,max}$ and its phase angle from 0° to 2π. The equivalent single-phase circuit of UPFC including two buses, a transmission line, the series and shunt voltage sources (V_{se} and V_{sh}), is shown in Fig. 2. The V_S and V_R could be any two buses of a power system in which the UPFC is installed.

Under the synchronous reference frame, the d-q axis components of the series and shunt controllers are used to generate the direct and quadrature components of the modulated voltages. The direct and quadrature components of the voltages are then used to generate the modulation index and phase shift for the PWM module. The d-q axis voltages of series and shunt converters can be expressed as

$$V_{sed} = m_{se} \cdot V_{dc} \cdot sin(\delta_{se} + \alpha_{se});\ V_{seq} = m_{se} \cdot V_{dc} \cdot cos(\delta_{se} + \alpha_{se}) \quad (11)$$

$$V_{shd} = m_{sh} \cdot V_{dc} \cdot sin(\delta_S + \alpha_{sh});\ V_{shq} = m_{sh} \cdot V_{dc} \cdot cos(\delta_S + \alpha_{sh}) \quad (12)$$

where δ_S and δ_{se} are the phase angle of bus voltage V_S and V_{se}. m_{se}, m_{sh}, α_{se} and α_{sh} are the modulation index and phase shift of series and shunt converters, respectively.

The real and reactive power of series and shunt converter (P_{se}, Q_{se}, P_{sh} and Q_{sh}), can be expressed as

$$P_{se} = |i_{se}|V_{dc}\, m_{se} cos(\alpha_{se});\ Q_{se} = |i_{se}|V_{dc}\, m_{se} sin(\alpha_{se}) \quad (13)$$

$$P_{sh} = |i_{sh}|V_{dc}\, m_{sh} cos(\alpha_{sh});\ Q_{sh} = |i_{sh}|V_{dc}\, m_{sh} sin(\alpha_{sh}) \quad (14)$$

where The series converter current $|i_{se}| = \left[(i_{sed}^2) + (i_{seq}^2)\right]^{1/2}$ and shunt converter current $|i_{sh}| = \left[(i_{shd}^2) + (i_{shq}^2)\right]^{1/2}$. i_{sed}, i_{seq}, i_{seh} and i_{shd} are the *d-q* axis currents of series and shunt converters, respectively.

The controller block for the series and shunt converters of UPFC are shown in Figs. 3(a) and (b). P_{se0}, Q_{se0}, P_{sh0} and Q_{sh0} are the initial values of real and reactive power for series and shunt converters. The m_{se}, α_{se}, m_{sh}, and α_{sh} are provided to the PWM generator, which generates the gating signals for the power electronic switches in the series and shunt converters. They obtained by m'_{se}, α'_{se}, m'_{sh}, and α'_{sh} by its 1st order lag process, respectively, which can be expressed as

$$\dot{m_{se}} = \frac{K_1}{T_1}(m'_{se} - m_{se});\ \dot{\alpha_{se}} = \frac{K_2}{T_2}(\alpha'_{se} - \alpha_{se}) \quad (15)$$

$$\dot{m_{sh}} = \frac{K_3}{T_3}(m'_{sh} - m_{sh});\ \dot{\alpha_{se}} = \frac{K_4}{T_4}(\alpha'_{sh} - \alpha_{sh}) \quad (16)$$

ISSN(Online): 2319 - 8753
ISSN (Print) :2347 - 6710

International Journal of Innovative Research in Science, Engineering and Technology

(An ISO 3297: 2007 Certified Organization)

Vol. 4, Issue 2, February 2015

and

$$m'_{se} = \frac{\sqrt{P_{se}^2+Q_{se}^2}}{V_{dc}\, i_{se}} \quad (17)$$

$$\alpha'_{se} = \cos^{-1}\frac{P_{se}}{\sqrt{P_{se}^2+Q_{se}^2}} \quad (18)$$

$$m'_{sh} = \frac{\sqrt{P_{sh}^2+Q_{sh}^2}}{V_{dc}\, i_{sh}} \quad (19)$$

$$\alpha'_{sh} = \cos^{-1}\frac{P_{sh}}{\sqrt{P_{sh}^2+Q_{sh}^2}} \quad (20)$$

where $P_{se}=P_{se0}+\Delta P_{se}$; $Q_{se}=Q_{se0}+\Delta Q_{se}$; $P_{sh}=P_{sh0}+\Delta P_{sh}$; $Q_{sh}=Q_{sh0}+\Delta Q_{sh}$. K_1~K_4 and T_1~T_4 are the gains and time constants of 1st order lag, respectively.

The ΔP_{se} and ΔQ_{se} are obtained from the ΔP_L and $\Delta V_S'$ via its 1st order lag process, respectively. The ΔP_L and $\Delta V_S'$ are the error signals of real power in the transmission line and bus voltage between the actual signals (P_L and V_S') and its reference signals (P_{Lref} and V_{Sref}'). The ΔP_{sh} and ΔQ_{sh} are obtained from the ΔV_{dc} and ΔV_S via its 1st order lag process, respectively. The ΔV_{dc} and ΔV_S are the error signals of dc link voltage and bus voltage between the actual signals (V_{dc} and V_S) and its reference signals (V_{dcref} and V_{Sref}). The ΔP_{se}, ΔQ_{se}, ΔP_{sh} and ΔQ_{sh} can be expressed as

$$\Delta\dot{P}_{se} = \frac{K_5}{T_5}(P_{Lref} - P_L);\ \Delta\dot{Q}_{se} = \frac{K_6}{T_6}\left(V'_{Sref} - V'_S\right) \quad (21)$$

$$\Delta\dot{P}_{sh} = \frac{K_7}{T_7}\left(V_{Sref} - V_S\right);\ \Delta\dot{Q}_{sh} = \frac{K_8}{T_8}\left(V_{dcref} - V_{dc}\right) \quad (22)$$

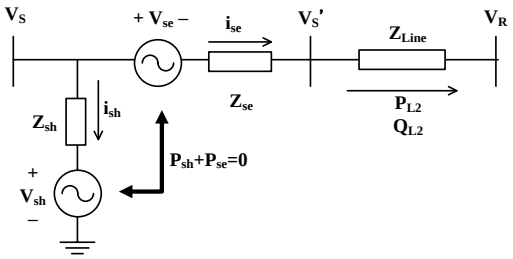

Fig. 2. The equivalent single-phase circuit of the UPFC

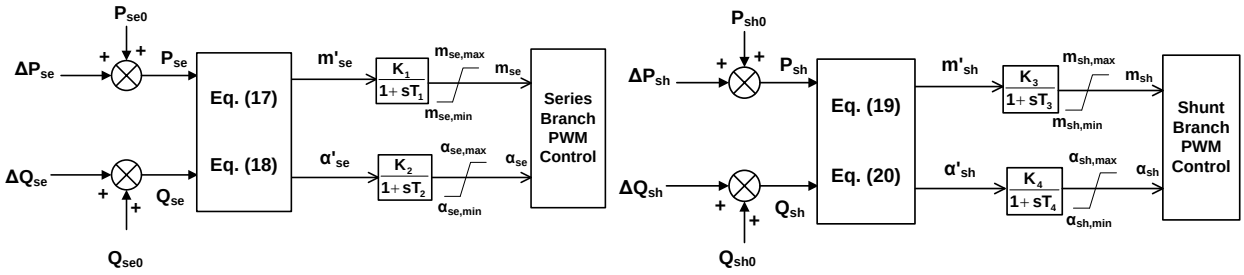

Fig. 3. The controller block of UPFC: (a) The series converter control block (b) The shunt converter control block

III. THE PROPOSED NIDC FOR UPFC

The proposed NIDC consists of three parts: the adaptive critic network, the FLENN and PID linear damping controller, as shown in Fig. 4. The designed NIDC provides the training signal $\Delta\alpha_{dam}$ to α_{sh} of the UPFC shunt converter to improve the OWF system stability. An FLNN is adopted to implement the function expansion for the FL-based ENN to improve the accuracy of the function approximation. The adaptive critic network [16], [17] is applied in order to provide suitable training signals for the FLENN controller. The FLENN produce the variation gains values (ΔK_P, ΔK_I and ΔK_D) of PID controller. The proposed NIDC is capable of providing near optimal results for complex and uncertain nonlinear system in order to solve the Hamilton–Jacobi–Bellman equation of optimal control [16], [17].

ISSN(Online): 2319 - 8753
ISSN (Print) :2347 - 6710

International Journal of Innovative Research in Science, Engineering and Technology

(An ISO 3297: 2007 Certified Organization)

Vol. 4, Issue 2, February 2015

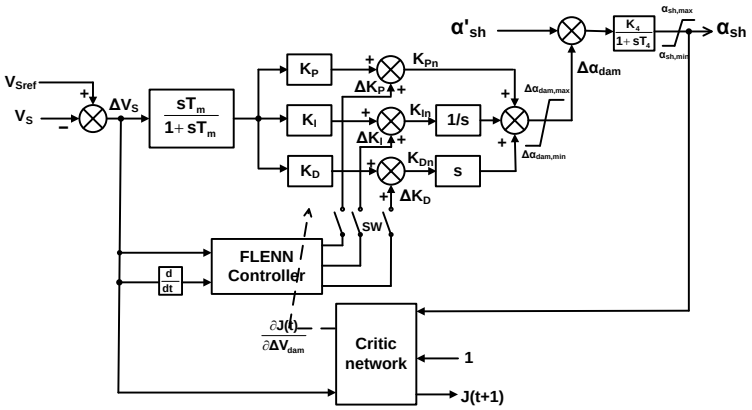

Fig. 4. Block diagram of proposed NIDC for UPFC

A. PID linear damping controller

The PID damping controller is analysis of complex eigenvalues based on a theory of modal control. The matrix of state space and the transfer function are follows as [18].

$$\dot{\mathbf{X}} = \mathbf{AX} + \mathbf{BR} \quad (23)$$

$$\mathbf{Y} = \mathbf{CX} + \mathbf{DR} \quad (24)$$

$$\mathbf{T(s)} = \mathbf{Y(s)/R(s)} \quad (25)$$

where $\mathbf{X}$ and $\dot{\mathbf{X}}$ are the state variables matrix and it's differential operator; $\mathbf{R}$ is the plant input matrix ΔV_S, Y corresponds to the system output $\Delta\alpha_{dam}$, as shown in Fig. 3. $\mathbf{A}$, $\mathbf{B}$, $\mathbf{C}$ and $\mathbf{D}$ are the constants of suitable system dimensions matrices. The substate vectors of $\mathbf{X} = [\mathbf{X_{wind}}, \mathbf{X_{UPFC}}, \mathbf{X_{SG}}, \mathbf{X_{AC}}]^T$, where $\mathbf{X}_{\text{wind}}$ is the state vector of PMSG-based wind farm, including dc link and electric system; $\mathbf{X}_{\text{UPFC}}$ is the state vector of UPFC; $\mathbf{X}_{\text{SG}}$ is the state vector of SG system, including excitation, turbine, governor and electromechanical system; $\mathbf{X}_{\text{AC}}$ is the state vector of transmission lines and buses system.

The winds peed is set 14 m/s for designing PID damping controller the UPFC, the transfer function T(s)[18] is represented as

$$\mathrm{T(s)} = \Delta\alpha_{dam}/\Delta V_S = {}^{sT_m}/_{1+sT_m}\left(K_P + {}^{K_I}/_{s} + sK_D\right) \quad (26)$$

where T_m is the time constant of the washout filter. K_P, K_I and K_D are the gains for PID controller.

The stable and unstable state can be found by complex eigenvalues λ_1-λ_{12} as shown in Table 1. It can be clearly to observe, most of the eigenvalues are fixed on the left side of the imaginary axis. The two sets eigenvalues $\boldsymbol{\lambda_4}$ and $\boldsymbol{\lambda_5}$ are close to the imaginary axis. Hence, from the column of with PID term of Table 1, the $\boldsymbol{\lambda_4}$ and $\boldsymbol{\lambda_5}$ of UPFC with PID controller have been prespecified and positioned in the appropriate place on the complex plane. From the column, all eigenvalues are seen to be stable. The $\boldsymbol{\lambda_4}$ and $\boldsymbol{\lambda_5}$ substituted to characteristic equation. The suitable values of K_P=-20.53, K_I=-27.6, K_D=7.51 and T_m=0.43 can be determined.

Table 1. The analysis of eigenvalues

Eigenvalues	without PID	with PID	Eigenvalues	without PID	with PID
λ_1	-3.856±35514	-3.856±35514	λ_7	-44.407±365.056	-44.407±365.056
λ_2	-5.738±356.98	-5.738±356.98	λ_8	-53.92±2957.635	-53.92±2957.635
λ_3	-72.66±320.6	-72.66±320.6	λ_9	-61.295±2289.215	-61.295±2289.215
$\boldsymbol{\lambda_4}$	***-1.446±3.509***	***-2.133±3.32***	λ_{10}	-112.67±1345.39	-112.67±1345.39
$\boldsymbol{\lambda_5}$	***-1.201±1.679***	***-1.748±0.883***	λ_{11}	-1.603±0.631	-1.821±1.353
λ_6	-1.516, -2.504	-1.529, -3.535	λ_{12}	-1.012, -1.0753	-1.012, -1.0753

B. FLENN

Fig. 5 shows the design of the FLENN. It has an input layer, a hidden layer with a sigmoid function $S(x)=1/(1+e^{-x})$, a context layer, and an output layer that is connected with an FLNN. The context layer is fed back to itself with a time delay z^{-1}. The FLNN uses a feedforward neural network structure to generate a set of linearly independent functions, and functionally expands the elements of the input variables. The trigonometric function is used in the FLNN, since it can be computed more quickly than the Gaussian, sine and cosine functions. The input vector $\boldsymbol{X}=[X_1, X_2]^T$, which is a

ISSN(Online): 2319 - 8753
ISSN (Print) :2347 - 6710

International Journal of Innovative Research in Science, Engineering and Technology

(An ISO 3297: 2007 Certified Organization)

Vol. 4, Issue 2, February 2015

functional expansion that uses a trigonometric polynomial basis function, can be written in the enhanced space as $\boldsymbol{\psi}=[\psi_1, \psi_2,\ldots\psi_p]=[1, X_1, sin(\pi X_1), cos(\pi X_1), x_2, sin(\pi X_2), cos(\pi X_2), X_1X_2]$, where X_1X_2 is the outer product term. Furthermore, the FLNN output is expressed by a linear sum of the yth node, as follows:

$$\hat{f}_y(k) = \theta\left(\sum_E \psi_E(x_i)\cdot w_{Ey}\right) \qquad E=1,2,\ldots,9 \text{ and } y=1,2,\ldots,9 \tag{27}$$

where $\hat{f}_y$ is the outer product term. w_{Ey} is the connective weight, and ψ_E is the function expansion output. θ is a set of basic functions.

The FLENN input $\boldsymbol{X}=[\Delta V_S, \Delta V_S']^T$ is used by the power system to directly transmit the numerical inputs to the next layer in this study. The context neurons of FLENN serve as memory units, as they store the hidden layer output signal. Therefore, the FLENN can employ the context neurons to increase dynamic characteristics of the network. The node output of the each layer of the FLENN and the superscripts present the layer-number of the output O, while the subscripts present the signal number of the related output, and these are given as follows.

$$O_i^{(1)}(t) = X_i^{(1)}(t);\ i=1,2 \tag{28}$$

$$O_j^{(2)}(t) = \sum_i O_i^{(1)}(t)\cdot w_{ij} + \sum_i O_r^{(3)} w_{rj}\ ;\ j = 1,2,\ldots,9 \tag{29}$$

$$O_r^{(3)}(t) = \alpha O_r^{(3)}(t-1) + O_j^{(2)}(t-1) \tag{30}$$

$$O_m^{(4)}(t) = \hat{f}_y \prod_{y=1}^{9} O_j^{(2)}(k)\cdot w_{jy} \tag{31}$$

$$O^{(5)}(t) = \sum_y O_y^{(4)}(k)\cdot w_o \tag{32}$$

where the w_{ij} is the connecting weights of the input layer to the hidden layer, while w_{rj} is the connecting weights of the context layer to the hidden layer. α is the self-connecting feedback gain (0~1) of context neurons, and w_{jy} is the connecting weight between the hidden layer and multiplication layer. The link weight w_o at output layer is unity. The objective of the FLENN controller is to train the parameters w_{ij}, w_{rj}, w_{jy} and w_{Ey} to make the best match with regard to the control signal $O^{(5)}$ to generate ΔK_P, ΔK_I and ΔK_D.

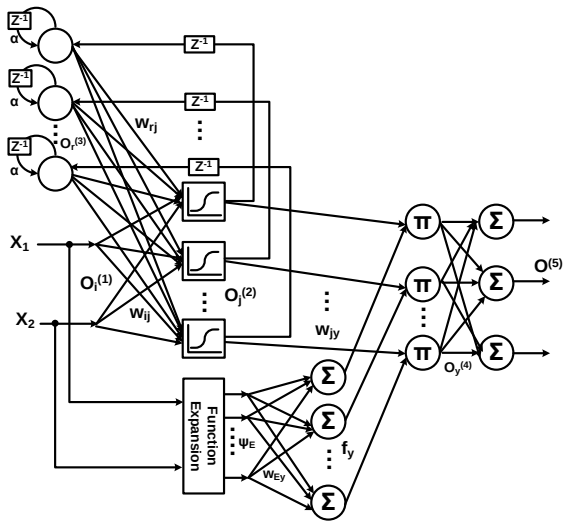

Fig. 5. FLENN controller

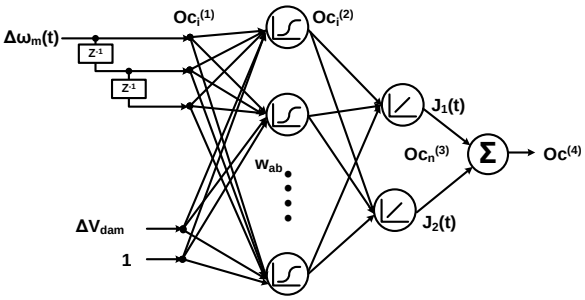

Fig. 6. Critic network

C. Critic network

A critic network can be continuously trained forward in order to learn the cost-to-go function associated with the power system. This ability is of great importance for real time optimal control operations when there are changes in configuration and operating conditions. The cost-to-go function J of Bellman's equation of dynamic programming estimated by the critic network is as follows [14].

$$J(t) = \sum_{k=0}^{\infty}\gamma^k U(t+k) = U(t) + \sum_{k=0}^{\infty}\gamma^k U[(t+1)+k] = U(t) + \gamma\cdot J(t+1) \tag{33}$$

where the utility function $U(t)$ is an important effect to form the optimal cost-to-go function. γrepresents the discount factor (0~1). The utility function of the critic network is $U(t)$, as follows.

$$U(t) = |\Delta V_S(t) + \Delta V_S(t-1) + \Delta V_S(t-2)| \tag{34}$$

The node output of the each layer of the critic network and the superscripts represent the layer-number of the output Oc, while the subscripts present the signal number of the related output, and these are given as follows.

ISSN(Online): 2319 - 8753
ISSN (Print) :2347 - 6710

International Journal of Innovative Research in Science, Engineering and Technology

(An ISO 3297: 2007 Certified Organization)

Vol. 4, Issue 2, February 2015

$$Oc_i^{(1)}(t) = X_i^{(1)}(t), \qquad \boldsymbol{X}=[\Delta V_S(t), \Delta V_S(t\text{-}1), \ldots 1],\ i=1,\ldots,4 \tag{35}$$

$$Oc_i^{(2)}(t) = \frac{1}{1+exp^{H}},\ H = \sum_{i=1}^{4} Oc_i^{(1)} \cdot w_{ab} \tag{36}$$

$$Oc_n^{(3)}(t) = J_n(t) = \sum_{n=1}^{2} Oc_i^{(2)}, n = 1,2 \tag{37}$$

$$Oc^{(4)}(t) = \sum Oc_n^{(3)} = J(t) \tag{38}$$

where w_{ab} is the connecting weights of the input layer to hidden layer.

Using Eq. (34), the UPFC should improve the performance of bus voltage deviation ΔV_S. The critic network in Fig. 6 has a four-layer feed-forward network structure. The training process ensures that the critic network provides optimal control to minimize the *J(t)*, which enables the FLENN controller to provide the optimal parameters of PID controller to the UPFC in this paper.

D. The training process of FLENN and critic network

The gradient of the error function is the direction to which the function increases. Therefore, searching the opposite side of the gradient can force the cost-to-go function to be minimized. The gradient descent algorithm with the mean squared error function as the error function *E* can be defined by [16]

$$E = 0.5[J^*(t) - J(t)]^2 = 0.5[U(t) + \gamma \cdot J^*(t+1) - J(t)]^2 \tag{39}$$

where the $J^*(t)$ is the reference value of the cost-to-go function, which in the case of dealing with deviation signals is zero.

The changes in direct proportion to the amount that weights w_{ab} are modified, and can be used to produce the instantaneous estimates of the negative gradient. In order to use an on-line algorithm for the critic network and proposed FLENN, the gradient based on the chain rule can be represented as (40) and (41). The formulae for adjusting the w_{ab} of the critic network and weights W_{FLENN} of FLENN are shown in by (42) and (43).

$$\frac{\partial E}{\partial w_{ab}} = \frac{\partial E}{\partial J} \cdot \frac{\partial J}{\partial w_{ab}} \tag{40}$$

$$\frac{\partial E}{\partial W_{FLENN}} = \frac{\partial E}{\partial J} \cdot \frac{\partial J}{\partial O^{(5)}} \cdot \frac{\partial O^{(5)}}{\partial W_{FLENN}} \tag{41}$$

$$w_{ab}(t+1) = w_{ab}(t) - \eta_{ab} \cdot \frac{\partial E(t)}{w_{ab}(t)} \tag{42}$$

$$W_{FLENN}(t+1) = W_{FLENN}(t) - \eta_{FL} \cdot \frac{\partial E(t)}{W_{FLENN}(t)} \tag{43}$$

where η_{ab} is the learning rate of w_{ab}. $W_{FLENN} = [w_{ij}, w_{rj}, w_{jy}, w_{Ey}]$, and $\eta_{FL} = [\eta_{ij}, \eta_{rj}, \eta_{jy}, \eta_{Ey}]$ are the learning rates of W_{FLENN}.

IV. CASE STUDIES AND SIMULATIONS

The proposed NIDC were simulated in this section. The damping controllers of SMIB plus the OWF system are compared with and without UPFC, with UPFC plus PID controllers while SW off, and with UPFC joined with the proposed NIDC while SW on in Fig. 4. The power system in Fig. 1 is simulated using PSCAD software, while the FLENN and critic network with GACO are achieved in a MATLAB 7.0 program. Three cases are described here to illustrate the proposed method.

Case A: The stability of changes in wind speed

The wind speed is assumed to change from 14 m/s to 11 m/sat the 10th second, from 10 m/s to 19 m/s at the 15th second and from 19 m/s to 14 m/s at the 17th second in Fig. 7(a). Figs. 7(b) and (c) show the responses of the real and reactive powers of Line 2, respectively. It is found that the real and reactive powers of the OWF change with the variations of wind speed. When the UPFC is in service, the amplitudes of the real and reactive power changes can be reduced, and thus better control is achieved. The smallest amplitude changes on the real and reactive powers of Line 2 can be obtained when the proposed NIDC is installed with the UPFC. Similar amplitude results can be found from the real and reactive powers of Line 1 shown in Figs. 8(a) and (b). Figs. 9(a) and (b) show the responses of the voltage magnitudes of Bus S and Bus R, respectively. When the wind

ISSN(Online): 2319 - 8753
ISSN (Print) :2347 - 6710

International Journal of Innovative Research in Science, Engineering and Technology

(An ISO 3297: 2007 Certified Organization)

Vol. 4, Issue 2, February 2015

speed changes, the voltage magnitudes of Bus S and Bus R can also be found at the desired level. The voltage magnitudes of the two buses have the smallest variations when the proposed NIDC is joined with the UPFC.

Case B: Transient stability of the three phase fault

A three-phase short circuit with a duration of 0.1secondis simulated at the 30th second. The fault is used to compare the damping characteristics of the proposed scheme. When a fault occurs, Figs. 10(a) and (b) show that the UPFC with a PID controller (green line) can have better damping performance with regard to the real and reactive power on Line2 than the system without UPFC (red line). It can be also seen that the proposed NIDC for UPFC (blue line) has the best damping effect on the transient stability for both real and reactive powers. Similar stability improvements can be also found from the transient stability of the real and reactive powers of Line 1 shown in Figs. 11(a) and (b). Figs. 12(a) and (b) also show that the UPFC with the NIDC can effectively improve the voltage transient stability of Bus S and Bus R. Fig. 12 (c) shows that the rotor speed of the wind PMSG (ω_r) can quickly recover to the corresponding steady state when the system has the UPFC installed with NIDC, with better results than are seen with the systems that have UPFC plus only PID controller and without UPFC.

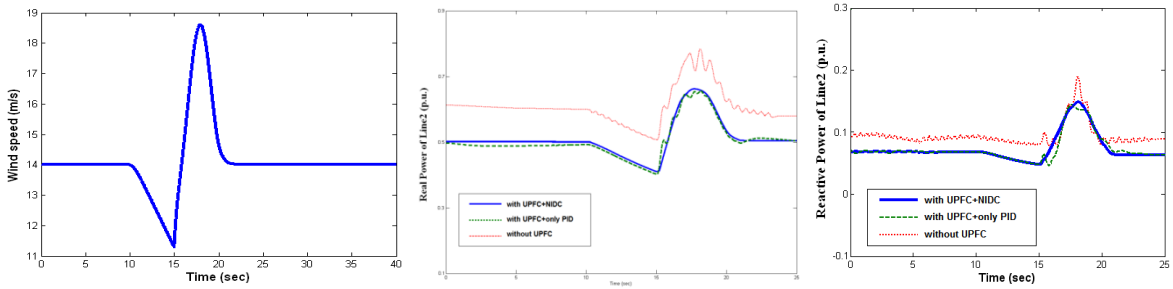

(a) (b) (c)

Fig. 7 The responses of the real power and reactive power of Line 2 when the wind speed changes. (a) wind speed response (b) P_{L2}. (c) Q_{L2}.

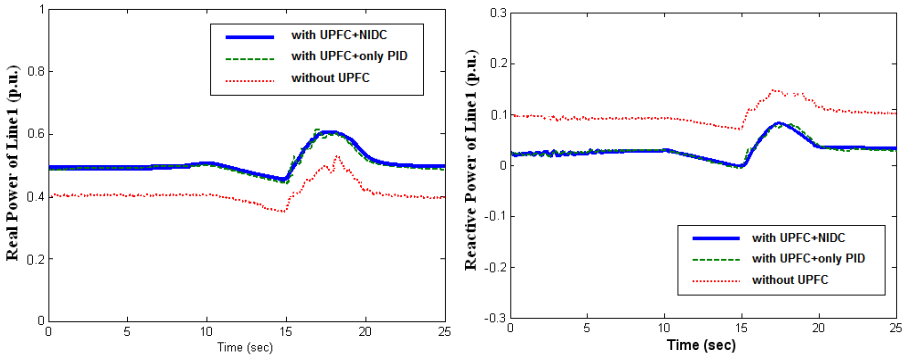

(a) (b)

Fig. 8 The responses of the real power and reactive power of Line 1. (a) P_{L1}. (b) Q_{L1}.

ISSN(Online): 2319 - 8753
ISSN (Print) :2347 - 6710

International Journal of Innovative Research in Science, Engineering and Technology

(An ISO 3297: 2007 Certified Organization)

Vol. 4, Issue 2, February 2015

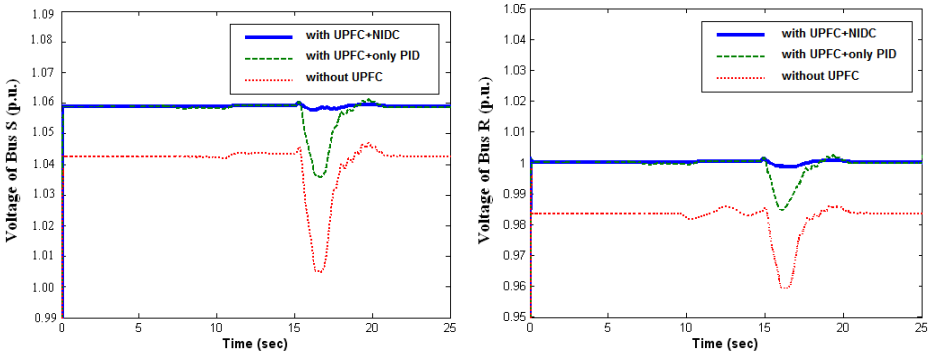

(a) (b)

Fig. 9 The responses of the voltage of Bus S and Bus R. (a) V_S. (b) V_R.

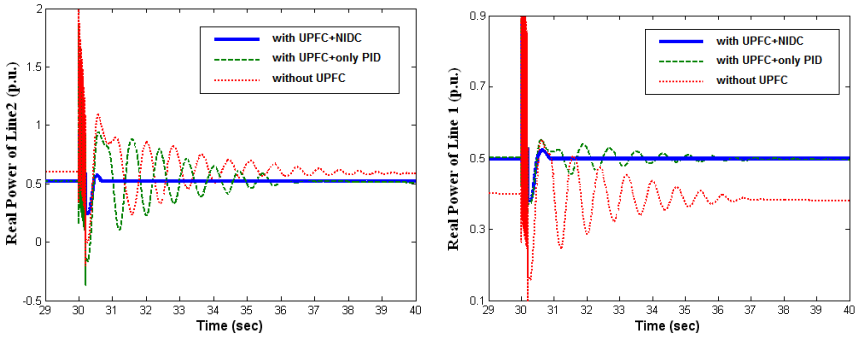

(a) (b)

Fig. 10 The responses of the real power and reactive power of Line 2 when the fault occurs. (a) P_{L2}. (b) Q_{L2}.

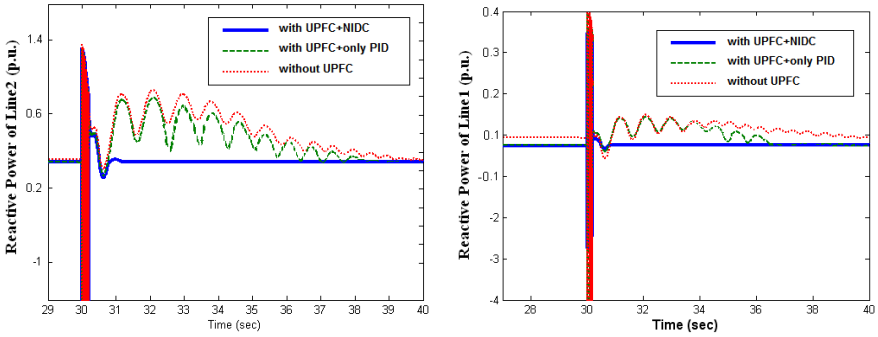

(a) (b)

Fig. 11 The responses of the real power and reactive power of Line 2 when the fault occurs. (a) P_{L1}. (b) Q_{L1}.

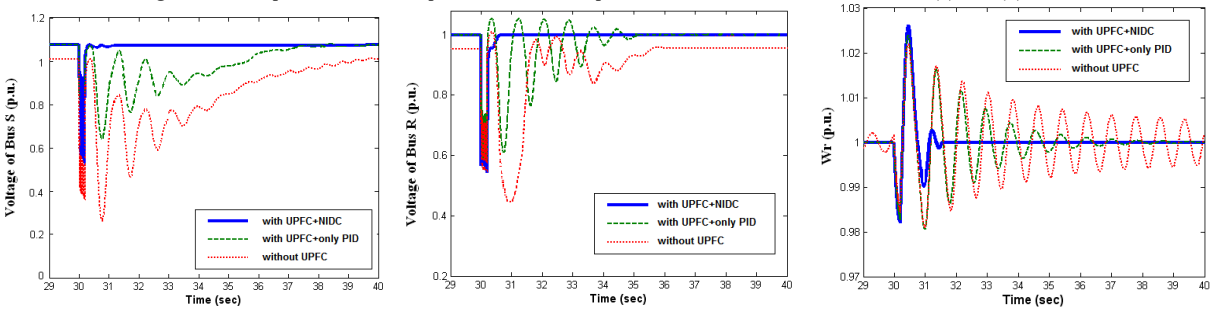

(a) (b) (c)

Fig. 12 The stability of the voltage of Bus S and Bus R and rotor speed of wind PMSG when the fault occurs. (a) V_S. (b) V_R. (c) ω_r

V. CONCLUSION

ISSN(Online): 2319 - 8753
ISSN (Print) :2347 - 6710

International Journal of Innovative Research in Science, Engineering and Technology

(An ISO 3297: 2007 Certified Organization)

Vol. 4, Issue 2, February 2015

The results reported in this paper demonstrate the effectiveness of the proposed designed PID controller and NIDC for a UPFC with regard to improving the power control and stability of a grid containing a large-scale OWF and SG. The transient responses of the studied system subject to a three-phase short circuit fault show the effectiveness of the proposed method. Moreover, the online learning algorithms of the connective weights deviations of proposed FLENN and critic network were derived in this work. The control performance of the proposed NIDC shows that the method presented in this work can effectively stabilize the network under unstable conditions.

APPENDIX

The parameters of the system examined in this paper are set as follows

(1). SG and single machine infinite bus:
S=1230MVA, V=15KV, PF=0.975 lagging, R_{L1}=R_{L2}=0 pu, X_{L1}=0.6 pu, X_{L2}=0.4 pu, R_{SG}=0 pu, X_{SG}=0.0012 pu, f=60Hz, T_1= 15/161KV, T_2=23/161KV

(2). PMSG-based OWF:
P_m = 750 W; 3.75 A; 3000 r/min, ρ= 1.25 kg/m3; r = 0.5 m; J= 1.32×10^{-3}Nms^2, B= 5.78×10^{-3} Nm s/rad

(3). UPFC with control system:
S_{upfc}=160 MVA, V=161KV, R_{se}=R_{sh}=0.01pu, X_{se}=X_{sh}=0.1pu, K_1=15, K_2=15, K_3=1, K_{p4}=01, T_1=0.15, T_2=0.1, T_3=0.5, T_4=0.2

(4). FLENN and critic network:
P=15, d=5, initial learning rates η_{ij}=0.51, η_{rj}=0.52, η_{jy}=0.72, η_{Ey}=0.51 and η_{ab}=0.35, τ_0 = 3000, γ=1, β=2, ρ = 0.085, d=5, crossover rate=0.05, mutation rate=0.08

REFERENCES

[1] Shariatpanah H., Fadaeinedjad R., and Rashidinejad,M. "A New Model for PMSG-Based Wind Turbine With Yaw Control", IEEE Energy Convers., vol. 28, no. 4, pp 929-937, 2013
[2] Senjyu T., Sakamoto R., Urasaki N., Funabashi T., and Sekine H., "Output power leveling of wind farm using pitch angle control with fuzzy neural network"', in Proc. Power Eng. Soc. Gen. Meeting., Jun. 2006.
[3] Sakamoto R., Senjyu T., Kaneko T., Urasaki N., Takagi T., Sugimoto S., and Sekine H., "Output power leveling of wind turbine generator by pitch angle control using $H\infty$ control", IEEE Trans. Power Syst., pp 2044-2049, 2006.
[4] Lin W. M., Hong C. M., Ou T. C., and Chiu T. M., "Hybrid intelligent control of PMSG wind generation system using pitch angle control with RBFN", Energy Convers. and Mana., vol. 52, no.2, pp 1244-1251, 2011
[5] Hingorani N. G. and Gyugyi L., "Understanding FACTS, Concepts and Technology of Flexiable AC Transmission Systems". IEEE Power Engineering Society and CIGRE, "FACTS overview" IEEE publication No. 95 TP 108, 1995.
[6] Farrag M. E. A., and Putrus G. A., "Design of an Adaptive Neurofuzzy Inference Control System for the Unified Power-Flow Controller", IEEE Trans. Power Del., vol.27, no.1, pp 53-61, 2012.
[7] Ajami A., M.Shotorbani A., and M Aagababa. P., "Application of the direct Lyapunov method for robust finite-time power flow control with a unified power flow controller", IET Gener. Transm. Distrib., vol.6, no.9, pp 822-830, 2012.
[8] Malhotra U., and Gokaraju R., "An Add-On Self-Tuning Control System for a UPFC Application", IEEE Trans. Industrial Electronics, vol.61, no.5, pp 2378-2388, 2014
[9] Mehraeen S., Jagannathan S., and row C M. L., "Novel Dynamic Representation and Control of Power Systems With FACTS Devices", IEEE Trans. Power Syst., vol.25, no.32, pp 1542-1554, 2010
[10] Shayeghi H., Shayanfar H., Jalilzadeh S., and Safari A., "Design of output feedback UPFC controller for damping of electromechanical oscillations using PSO", Energy Convers., vol. 50, no. 10, pp 2554-2561, 2009
[11] Seethalekshmi K., Singh S. N., and Srivastava S. C., "Synchrophasor Assisted Adaptive Reach Setting of Distance Relays in Presence of UPFC", IEEE Systems Journal, vol.5, no.3, pp 396-405, 2011
[12] Lin W. M., Hong C. M., Huang C. H., and Ou T. C., "Hybrid Control of a Wind Induction Generator Based on Grey–Elman Neural Network", IEEE Trans. Control Systems Tech., vol. 21, no. 6, pp 2367–2373, 2013
[13] Toh K. A. and Yau W. Y., "Fingerprint and speaker verification decisions fusion using a functional link network," IEEE Trans. Syst., Man, Cybern. C, Appl. Rev., vol. 35, no. 3, pp. 357–370, Aug. 2005.
[14] Chaturvedi K. T., and Pandit M., and Srivastava L., "Self-Organizing Hierarchical Particle Swarm Optimization for Nonconvex Economic Dispatch", IEEE Trans. Power Syst., vol. 23, no. 3, pp 1079-1087, 2008
[15] Trilla, L., Bianchi, F. D., Gomis-Bellmunt, O.; 'Linear parameter varying control of permanent magnet synchronous generators for wind power systems', IET Power Electr., 2014, 7, (3), pp 692-704
[16] Swaksharand R., and Ganesh K. V., "Wide-Area Signal-Based Optimal Neurocontroller for a UPFC", IEEE Trans. Power Del., vol. 2, no. 3, pp 1597-1605, 2008
[17] Xu X., Hou Z., Lian C., and He H., "Online Learning Control Using Adaptive Critic Designs With Sparse Kernel Machines", IEEE Trans. Neu. Net. and Lear. Syst., vol. 24, no. 5, pp. 762-775, 2013
[18] Fan L. and Miao Z., "Mitigating SSR Using DFIG-Based Wind Generation", IEEE Trans. Sust. Ener., vol. 3, no.3, pp. 2297-2302, 2012

ISSN(Online): 2319 - 8753
ISSN (Print) :2347 - 6710

International Journal of Innovative Research in Science, Engineering and Technology

(An ISO 3297: 2007 Certified Organization)

Vol. 4, Issue 2, February 2015

BIOGRAPHY

Whei-Min Lin (M'87) was born October 3rd, 1954. He received his BS-EE from the National Chao-Tung University, Hsin-Chu, Taiwan, and the MS-EE from the University of Connecticut, Storrs, and the Ph.D. degree in electrical engineering from the University of Texas, Arlington, in 1985. He joined Control Data Corporation in 1986, Minneapolis, MN, and worked with Control Data Asia, Taipei, Taiwan, in 1989. He has been with National Sun Yat-Sen University, Kaohsiung, Taiwan, since 1991. Dr. Lin's interests are GIS, Distribution system, SCADA and automatic control system. Dr. Lin is a member of IEEE and Tau Beta Pi.

Kai-Hung Lu was born on July 21, 1979. He received the B.S. degree in the department of Electronic Engineering from Kao Yuan University, Kaohsiung, Taiwan, in 2001 and the M.S. degree in the department of Electrical Engineering, National United University, Miaoli, Taiwan, in 2006. He is working for his Ph.D degree in the department of Electrical Engineering, National Sun Yat-Sen University, Kaohsiung, Taiwan. His research interests include high capacity power electronic systems, power system operation, power system security, neural networks, UPFC and new FACTS devices.